International Journal of Solids and Structures 206 (2020) 236–246

Contents lists available at ScienceDirect

International Journal of Solids and Structures

journal homepage: www.elsevier.com/locate/ijsolstr

Analytical solution of the peak bending moment of an M boom for membrane deployable structures

Hui Yang [a], Hongwei Guo [b], Yan Wang [a,*], Jian Feng [a], Dake Tian [c]

[a] College of Electrical Engineering and Automation, Anhui University, Hefei 230601, China
[b] State Key Laboratory of Robotics and System, Harbin Institute of Technology, Harbin 150001, China
[c] School of Mechanical Engineering, Shenyang Jianzhu Univesity, Shenyang 110168, China

ARTICLE INFO

Article history:
Received 18 May 2020
Received in revised form 22 August 2020
Accepted 4 September 2020
Available online 13 September 2020

Keywords:
Self-deployable structure
Thin-walled boom
Nonlinear deformation
Analytical solution
Experiment

ABSTRACT

A deployable M cross section thin-walled boom (M boom) can be flattened and coiled elastically around a hub; and can then be self-deployed by releasing the stored strain energy. The M boom has been proposed as the key member of membrane deployable structures. First, the covariant base vectors of geometrical relation of the single type I tape spring were analyzed by establishing three coordinate systems. Second, the constitutive relation between stress and strain was expressed according to the Kirchhoff-Love hypothesis. Third, the equilibrium and controlling equations of the single tape spring were modeled based on Calladine shell theory. Fourthly, the total strain energy model of the single type I tape spring was built by integration. Fifth, the strain energy of the M boom was modeled by the sum of the strain energies of the six tape springs. Then, the strain energies of the single type II and III tape springs were analyzed. The sum of the strain energies of the six tape springs equals the total strain energy of the M boom. The bending moment model was established based on the minimum potential energy principle. The experimental equipment and four M boom samples were processed. The bending force value of the M booms was tested 20 times. Then, the average peak bending moment was calculated. The relative error between the theoretical and experimental results of the peak bending moment does not exceed 6.5% verifying the accuracy of the theoretical model.

1. Introduction

Deployable thin-walled boom can be flattened and coiled elastically around a hub; and can then be self-deployed by releasing stored strain energy. M cross section thin-walled booms (M booms) have high specific rigidity and deploying-to-coiling ratio; and have thus been proposed as members of deployable structures, such as antennae, solar sail, and drag sail. A 108-m deployable space antenna was proposed and tested under the Innovative Space Based Radar Antenna Technology program with thin-walled hinges (Lane et al., 2011). NanoSail-D with four triangular rollable and collapsible (TRAC) booms was a subscale sail system designed for small spacecraft applications (Johnson et al., 2011). An advanced flexible blanket ROSA with two C cross section booms (C booms) was developed by deployable space systems (Hoang et al., 2016).

The gossamer sail system with a 5 m × 5 m square solar/drag sail for deorbiting in low earth orbit; was designed and developed using four bistable carbon fibers lenticular booms (Fernandez et al, 2014). The flattening process of deployable lenticular boom under compression and tension was studied (Hu et al., 2017). A retractable/deployable mechanism with a lenticular boom was proposed and its dynamic properties were analyzed (Chu and Lei, 2014). A thin-walled lenticular boom was fabricated by vacuum-bag and co-bonding technology and folding analysis was performed (Bai et al, 2019).The force that a C boom can exert before blossoming occurs by using the strain energy stored in the coiled boom and in the compression springs was predicted and tested (Hoskin et al., 2017). The folding and deployment of tape spring and tubular booms with integrated folding hinges to smoothen the folding have been investigated by several authors (Seffen and Pellegrino, 1999; Mallikarachchi and Pellegrino, 2014a, 2014b). The responses of C boom as a representative thin-walled flexible structure under static and vibrational loading were studied (Oberst et al., 2018). An ultra-thin carbon fiber deployable TRAC boom subjected to two bending conditions was optimized to increase the ultimate buckling loads (Bessa and Pellegrino, 2018). Wrapping dynamic analysis and optimization were performed on a composite TRAC boom to increase the peak moment and reduce the stress concentration by the response surface method (Yang et al., 2018, 2019).

* Corresponding author at: Room 334, Ligong Building A, No.111, ST. Jiulong, Dist. Jingkai, Hefei, China
E-mail addresses: huiyang_0431@163.com (H. Yang), guohw@hit.edu.cn (H. Guo), wangyan_597@163.com (Y. Wang), wnwhheart@163.com (J. Feng), tiandake@sjzu.edu.cn (D. Tian).

https://doi.org/10.1016/j.ijsolstr.2020.09.005
0020-7683/

The structural characteristics of a bi-convex boom were described, and the effect of the braid mesh's tension on the stiffness of the boom was investigated by the analytical method (Miyazaki et al., 2015). Although the bending stiffness of the TRAC boom is high, its torsional stiffness is much lower than those of other kinds of thin-walled deployable boom. This article proposes an M cross section boom that consists of four tape springs bonding along one longitudinal edge, and the four tape springs are mirror-symmetric. The arc and a straight line are tangent on the cross-section of the two outer side tape springs. One end of the two arcs on the cross-section of the two inner side tape springs are inverse tangent, and the other end of the arc is tangent to the straight line. M boom has a greater torsional stiffness than TRAC boom.

M booms have a strong self-extensibility, which is an important behavior in deployable structures. Fig. 1 illustrates an example of two self-deployable membrane structures using M booms. The booms support the membrane when deployed, and the deployable structure can be folded in a small volume. The deployable structures do not require additional deriving motor because of the self-deploying property of M booms. Thus M booms are quite suitable for use in membrane antennae; and solar and drag sails.

The buckling moment of M booms represents the resistance capacity of deployable structures in the full deployment state. However, few research has derived the buckling moment of M booms theoretically. The buckling moment equals the peak bending moment. Thus, the deformation of a single tape spring is analyzed, and the bending moment of the M boom is then derived. In addition to the analytical solution, parametric studies are performed to investigate the effects of the section radius, the central angle, the thickness, and the curvature on the peak bending moment.

Section 2 derives the deformation of a single type I tape spring. The geometrical relation is established in Section 2.1, the strain energy is derived in 2.2, and the equilibrium equations are derived in Section 2.3, and the bending moment is presented in Section 2.4. Section 3 derives the deformation of one type II or III tape spring. Section 4 derives the bending of six tape springs in the M boom. Experimental evaluation is provided in Section 5. Finally, the concluding remarks are presented in Section 6.

2. Deformation of a single type I tape spring

The geometric diagram of the M boom is shown in Fig. 2. The M boom consists of four tape springs bonding along one longitudinal edge, and the four tape springs are mirror-symmetric. The M boom can be flattened and coiled elastically and self-deploy by releasing stored strain energy around a hub. The M boom consists of three type tape springs, namely, types I, II, and III, as shown in Fig. 2. The type I tape springs with central angle ϕ_1 are located inside the boom, whose bonded web is at the center of the symmetrical line of the cross section. The type II tape spring with central angle ϕ_1 is tangent to the arc in reverse, and the type III tape springs with central angle ϕ_2 are located outside the boom. The offset distance of the type II tape spring from the central symmetrical line is s. The height of the three bonded webs is l, and the thickness of the four tape springs is t. An analytical solution of the local deformation of a single type I tape spring under bending is derived in this section.

2.1. Geometrical relation

The single tape spring under bending is shown in Fig. 3. The orthogonal coordinate system (x, y, z) and the corresponding orthonormal base vector ($\boldsymbol{E}_x$, $\boldsymbol{E}_y$, $\boldsymbol{E}_z$) are set up, where $0 \le x \le l$, $-R\Phi/2 \le y \le R\Phi/2$, and $-t/2 \le z \le t/2$. The inertial Cartesian frame is denoted as O-$\boldsymbol{i}_1$-$\boldsymbol{i}_2$-$\boldsymbol{i}_3$. The x-axis is parallel to $\boldsymbol{i}_1$, and the y-axis is along the section curve of the tape spring (Fukunaga and

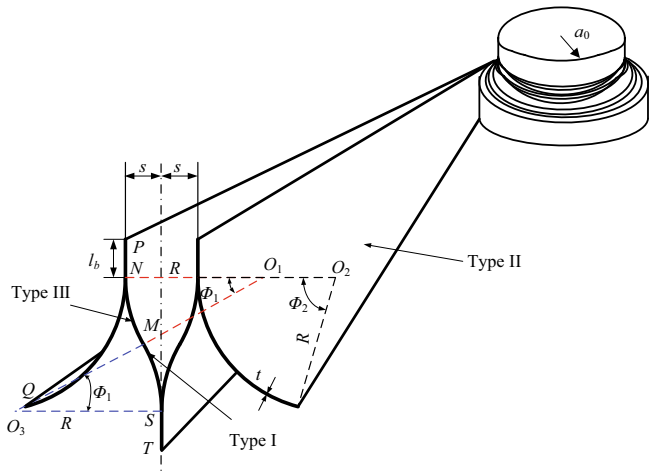

Fig. 2. Geometric diagram of the M boom.

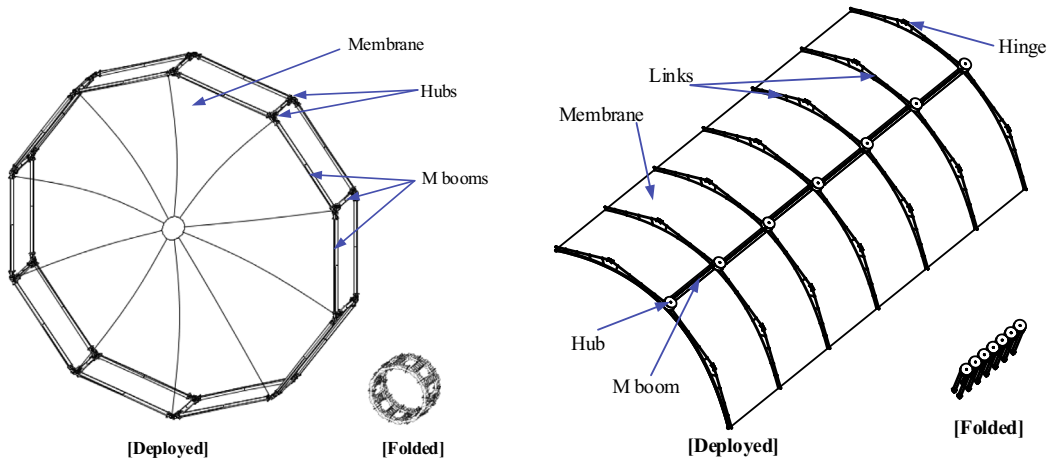

(a) One hoop deployable mechanism (b) One parabolic cylindrical deployable truss.

Fig. 1. Self-deployable boom-membrane structure.

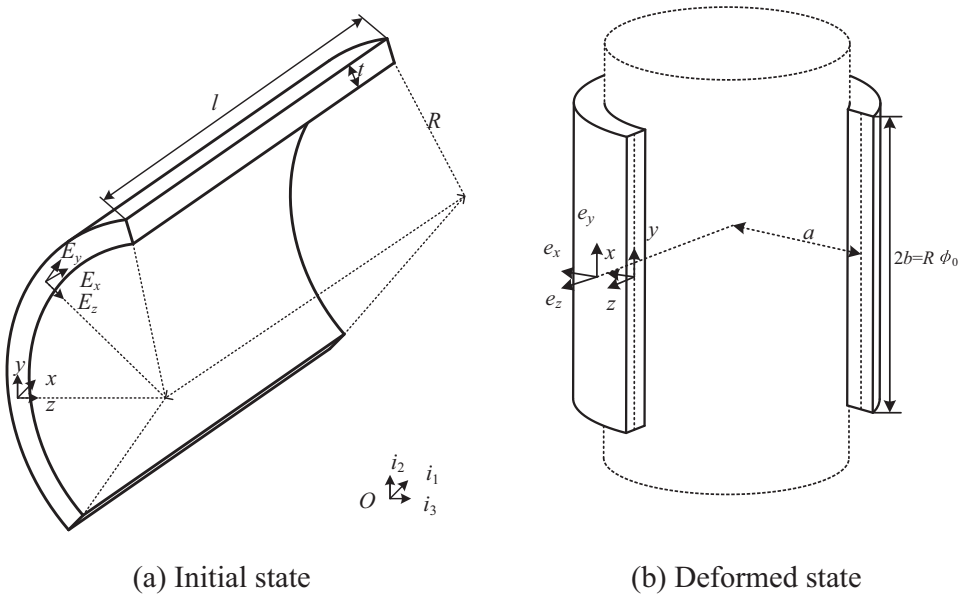

(a) Initial state (b) Deformed state

Fig. 3. The single type I tape spring under bending.

Miyazaki, 2018). The relation between ($\boldsymbol{E}_x$, $\boldsymbol{E}_y$, $\boldsymbol{E}_z$) and ($\boldsymbol{i}_1$, $\boldsymbol{i}_2$, $\boldsymbol{i}_3$) is derived as follows:

$$E_x = i_1,\ E_y = \cos\left(\frac{y}{R}\right)i_2 + \sin\left(\frac{y}{R}\right)i_3,\ E_z = -\sin\left(\frac{y}{R}\right)i_2 + \cos\left(\frac{y}{R}\right)i_3 \quad (1)$$

where R is the cross sectional radius of the four tape springs.

The position vector of an arbitrary point in the thin walled shell in the initial state is given as

$$X = (z - R)E_z + x\mathbf{i}_1 \quad (2)$$

Combined with Eq. (2), the covariant base vectors $\boldsymbol{G}_x$, $\boldsymbol{G}_y$ and $\boldsymbol{G}_z$ along the x-, y-, and z axes in the initial state are expressed as

$$G_x = \frac{\partial X}{\partial x} = i_1,\ G_y = \frac{\partial X}{\partial y} = (1 - k_0 z)E_y,\ G_z = \frac{\partial X}{\partial z} = E_z \quad (3)$$

where k_0 is the initial curvature of the single tape spring, that is, $k_0 \equiv 1/a_0$.

The tape spring is subject to the opposite-sense bending of radius a as shown in Fig. 4(b). The coiling deformed state is shown in Fig. 2 (b). The axis of the hub is along the direction of the y-axis. Orthonormal base vector (x, y, z) is denoted as (e_x, e_y, e_z), and the y-axis is parallel to i_2. The relation between (e_x, e_y, e_z) and $(\boldsymbol{i}_1, \boldsymbol{i}_2, \boldsymbol{i}_3)$ is derived as

$$\begin{aligned} e_x &= \cos\left(\frac{x}{a} - \frac{l}{2a}\right)i_1 - \sin\left(\frac{x}{a} - \frac{l}{2a}\right)i_3 e_y = i_2 \\ e_z &= +\sin\left(\frac{x}{a} - \frac{l}{2a}\right)i_1 + \cos\left(\frac{x}{a} - \frac{l}{2a}\right)i_3 \end{aligned} \quad (4)$$

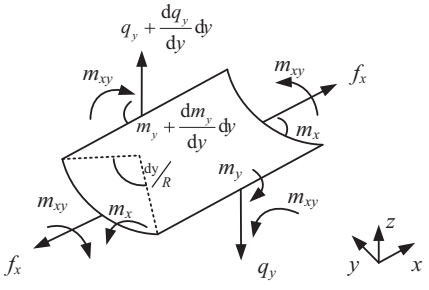

Fig. 4. Stress resultants in a typical element of the single tape spring.

where a is the radius of the bending circle, and l is the length of the tape spring as shown in Fig. 2(a).

The displacement of the single tape spring from the bending state in the relative axis is (u, v, w), that is, (u, v, w) is the displacement along (x, y, z). On the basis of the Kirchhoff-Love hypothesis, the position vector x in the bending deformed state is given as

$$x = x_0 + \frac{z}{\left|\frac{\partial x_0}{\partial x} \times \frac{\partial x_0}{\partial y}\right|}\frac{\partial x_0}{\partial x} \times \frac{\partial x_0}{\partial y} \quad (5)$$

where $\boldsymbol{x}_0$ is the position vector of the mid-surface ($z = 0$) of the single tape spring, that is,

$$x_0 = ue_x + (y + v)e_y + (a + w)e_z \quad (6)$$

The following conditions are assumed: (1) u is a function of x, while v and w are functions of y; (2) compared to initial radius R, the thickness t of the single tape spring is adequately small, that is, $zk \leqslant 1$.

Then, the position vector in the deformed state is derived as

$$\begin{aligned} x = {} & u(x)e_x + [y + v(y)]e_y + \left[\frac{1}{k} + w(y)\right]e_z \\ & + z[e_z + ku(x)e_x - w'(y)e_y] \end{aligned} \quad (7)$$

where k is the curvature of the single tape spring in the deformed state, $k \equiv 1/a$.

Substituting Eqs.(7) into (3), covariant base vectors $\boldsymbol{g}_x$, $\boldsymbol{g}_y$, and $\boldsymbol{g}_z$ are expressed as

$$\begin{cases} g_x = \frac{\partial x}{\partial x} = (1 + \dot{u} + kw + kz)e_x - kue_z \\ g_y = \frac{\partial x}{\partial y} = (1 + v' - zw'')e_y + w'e_z \\ g_z = \frac{\partial x}{\partial z} = e_z + kue_x - w'e_y \end{cases} \quad (8)$$

where the dot denotes the differentiation along x.

2.2. Strain and stress

Only axial stains can be observed along the x-, y-, and z- axes. The other strains vanish because of the symmetry of the deformation as shown in Fig. 2. According the assumed condition in Section 2.1, the second- or higher- order term of t/R of the strain is

negligible. The strains (ε_{xx} and ε_{yy}) along the x- and y- axes are derived as Eq.(9):

$$\varepsilon_{xx} = \frac{|g_x|}{|G_x|} - 1 = \sqrt{(1+\dot{u}+kw+kz)^2+(ku)^2} - 1 \approx \dot{u} + k(w+z) \tag{9}$$

$$\varepsilon_{yy} = \frac{|g_y|}{|G_y|} - 1 = \frac{\sqrt{(1+v'-zw'')^2+(w')^2}}{1-k_0 z} - 1 \approx v' + z(k_0 - w'') \tag{10}$$

Considering the orthotropic linear plain stress field in the orthonormal coordinate along the embedded coordinates (x, y, z), the constitutive relation between stress and strain can be expressed as

$$\sigma^{xx} = \frac{E_x}{1-v_x v_y}(e_{xx} + v_y e_{yy}) \tag{11}$$

$$\sigma^{yy} = \frac{E_y}{1-v_x v_y}(e_{yy} + v_x e_{xx}) \tag{12}$$

where E_x and E_y are the elasticity moduli along the x- and y-axes, respectively; and v_x, and v_y are the Poisson's ratios along the x- and y- axes, respectively.

2.3. Equilibrium equations

The stress resultants in a typical element of the single tape spring are shown in Fig. 4. On the basis of Calladine shell theory, by solving the force along the z- axis and the moment around the x- axis, two equations are derived as

$$\sum F_z = \frac{dq_y}{dy} - kF_x = 0 \tag{13}$$

$$\sum M_x = \frac{dM_y}{dy} - q_y = 0 \tag{14}$$

where F_x and F_z are the forces per unit length along the x- and z-axes, respectively; M_x and M_y are the bending-stress moments per unit length around the x- and y- axes, respectively; and q_y is the stress along the y- axis.

By combining Eq.(13) and Eq.(14), the shell equilibrium equation is derived by eliminating q_y.

$$\frac{d^2 M_y}{dy^2} + kF_x = 0 \tag{15}$$

According to the definition, the following equations are provided

$$\begin{cases} F_x = \int_{-t/2}^{t/2} \sigma^{xx}(1-k_0 z)dz; \\ F_y = \int_{-t/2}^{t/2} \sigma^{yy}(1-k_0 z)dz; \\ N_y = \int_{-t/2}^{t/2} z\frac{\partial \sigma^{yy}}{\partial y}(1-k_0 z)dz; \\ M_x = \int_{-t/2}^{t/2} z\sigma^{xx}(1-k_0 z)dz; \\ M_y = \int_{-t/2}^{t/2} -z\sigma^{yy}(1-k_0 z)dz; \end{cases} \tag{16}$$

where N_y is the stress resultants along the y-axis, σ^{xx} and σ^{yy} are the stresses along the x- and y- axes.

Substituting from yjorgottrh Eqs. (9)–(12) into Eq. (16), the following equations are obtained.

$$F_x = \frac{E_x t}{1-v_x v_y}(\dot{u} + kw + v_y v') - D_x k_0[k + v_y(k_0 - w'')] = v_x F_y + E_x t\left(\dot{u} + kw - \frac{t^2 k_0}{12}k\right) \tag{17}$$

$$F_y = \frac{E_x t}{1-v_x v_y}[v' + v_x(\dot{u} + kw)] - D_y k_0(v_x k + k_0 - w'')) \tag{18}$$

$$N_y = -\frac{\partial M_y}{\partial y} = -\widetilde{D}_y w''' \tag{19}$$

$$M_x = D_x[k_0(\dot{u} + kw + v_y v') + k + v_y(k_0 - w'')] = -\frac{t^2 k_0}{12}F_x + \widetilde{D}_x[k + v_y(k_0 - w'')] \tag{20}$$

$$M_y = -D_y\{v_x k + k_0 - w'' - k_0[v' + v_x(\dot{u} + kw)]\} = \frac{t^2 k_0}{12}F_y - \widetilde{D}_y(v_x k + k_0 - w'') \tag{21}$$

where

$$D_x = \frac{E_x t^3}{12(1-v_x v_y)}, \quad \widetilde{D}_x = D_x\left(1 - \frac{t^2 {k_0}^2}{12}\right),$$
$$D_y = \frac{E_y t^3}{12(1-v_x v_y)}, \quad \widetilde{D}_y = D_y\left(1 - \frac{t^2 {k_0}^2}{12}\right)$$

Given the orthotropic material of the single tape spring, the following equations are established

$$E_y = v_y E_x, \; v_x D_y = v_y D_x \; v_x \widetilde{D}_y = v_y \widetilde{D}_x \tag{22}$$

The single tape spring is in the pure bending deformed state. Thus, the boundary conditions are expressed as

$$F_y(\pm b) = 0 \; M_y(\pm b) = 0 \tag{23}$$

Given that u is a function of x, w is a function of y, and M_y is a constant. Eq. (21) leads to

$$\dot{u} = const. \equiv \alpha_{x0} \tag{24}$$

where α_{x0} is a constant.

By substituting Eqs. (17), (20), (23), and (24) into shell equilibrium equation Eq. (15), the following equation is derived

$$\widetilde{D}_y w'''** + E_x t k^2(w - w_0) = 0 \tag{25}$$

where $w_0 = \frac{t^2 k_0}{12} - \frac{\alpha_{x0}}{k}$.

Eq. (25) can be solved as

$$w = w_0 + bC_1 \cosh\eta\xi\cos\eta\xi + bC_2 \sinh\eta\xi\sin\eta\xi \tag{26}$$

where

$$\xi = \frac{y}{b}, \quad \eta = \sqrt[4]{\frac{E_x b^4 t k^2}{4\widetilde{D}_y}}$$

By combining Eqs. (19) and (21), boundary condition Eq. (23) can be expressed as

$$w''(b) = k_0 + v_x k, w'''(b) = 0 \tag{27}$$

By substituting Eqs. (27) into (26), C_1 and C_2 are eliminated, and the following equation is derived

$$w = \frac{t^2 k_0}{12} - \frac{\alpha_{x0}}{k} + \frac{b^2(k_0 + v_x k)}{3}(\chi_{11}\sinh\eta\xi\sin\eta\xi - \chi_{12}\cosh\eta\xi\cos\eta\xi) \tag{28}$$

where

$$\chi_{11}=\frac{3(\sinh\eta\cos\eta+\cosh\eta\sin\eta)}{\eta^2(\sinh2\eta+\sin2\eta)},$$
$$\chi_{12}=\frac{3(\cosh\eta\sin\eta-\sinh\eta\cos\eta)}{\eta^2(\sinh2\eta+\sin2\eta)}$$

2.4. Strain energy and bending moment

The strain energy π_I stored in the single type I tape spring is expressed as

$$\pi_I=\int_{-b}^{b}\int_{-t/2}^{t/2}\frac{1}{2}(\sigma^{xx}\varepsilon_{xx}+\sigma^{yy}\varepsilon_{yy})(1-k_0z)d_zd_y \tag{29}$$

where ε_{xx} and ε_{yy} are the strains along the x- and y- axes, respectively.

The strain energy per unit length includes two parts: the first part is the energy for deforming the initial tape spring shell into the flat plate, and the second part is the energy for bending the flat plate into a cylindrical shape around the hub with curvature k, that is,

$$\pi_I=\pi_{Ix}+\pi_{Iy} \tag{30}$$

Where π_{Ix} is the energy for deforming the initial tape spring shell into flat plate, $\pi_{Ix}=\frac{k}{2}\int_{-b}^{b}M_xd_y$; and π_{Iy} is the energy for bending the flat plate into a cylindrical shape, $\pi_{Iy}=-\frac{k_0}{2}\int_{-b}^{b}M_yd_y$.

By substituting Eqs.(20), (21) and (31) into Eq. (30), the following equation is derived:

$$\pi_I=b\widetilde{D}_x(1-v_xv_y)k^2+b\widetilde{D}_y(k_0+v_xk)^2(1-A_1) \tag{31}$$

On the basis of the minimum potential energy principle, bending moment M can be obtained as follows

$$M_I=\frac{d\pi_I}{dk} \tag{32}$$

By substituting Eqs. (31) into (32), the bending moment to be applied at the end of the single tape spring is derived as

$$M_I=2b\widetilde{D}_x(1-v_xv_y)k+2bv_x\widetilde{D}_y(k_0+v_xk)(1-A_1)-b\widetilde{D}_y(k_0+v_xk)^2\frac{A_4-A_1}{2k} \tag{33}$$

where

$$A_1=\frac{\cosh2\eta-\cos2\eta}{\eta(\sinh2\eta+\sin2\eta)},\quad A_4=\frac{4sinh2\eta\sin2\eta}{(\sinh2\eta+\sin2\eta)^2}$$

3. Bending of one type II or III tape spring in the M boom

The analytical solution of the local deformation of the single type II and III tape springs under bending are derived in this section. The single type II tape spring under bending is shown in Fig. 5.

3.1. Geometrical relation

The offset distance of the type II tape spring from the central symmetrical line is s. On the basis of the Kirchhoff-Love hypothesis, the position vector x in the bending deformed state is given as

$$x=x_0+\frac{z}{\left|\frac{\partial x_0}{\partial x}\times\frac{\partial x_0}{\partial y}\right|}\frac{\partial x_0}{\partial x}\times\frac{\partial x_0}{\partial y} \tag{34}$$

where

$$x_0=ue_x+(y+u)e_y+(a+w+s)e_z$$

By substituting Eqs. (34) into (3), covariant base vectors $\boldsymbol{g}_x$, $\boldsymbol{g}_y$ and $\boldsymbol{g}_z$ are expressed as

$$\begin{cases}g_x=\frac{\partial x}{\partial x}=(1+\dot{u}+kw+kz+ks)e_x-kue_z;\\ g_y=\frac{\partial x}{\partial y}=(1+v'-zw'')e_y+w'e_z;\\ g_z=\frac{\partial x}{\partial z}=e_z+kue_x-w'e_y\end{cases} \tag{35}$$

3.2. Strain energy and bending moment

By substituting Eqs. (35) into (3), the strain is derived as

$$\varepsilon_{xx}=\frac{|g_x|}{|G_x|}-1=\sqrt{(1+\dot{u}+kw+kz)^2+(ku)^2}-1\approx\dot{u}+k(w+z+s) \tag{36}$$

$$\varepsilon_{yy}=\frac{|g_y|}{|G_y|}-1=\frac{\sqrt{(1+v'-zw'')^2+(w')^2}}{1-k_0z}-1\approx v'+z(k_0-w'') \tag{37}$$

By substituting Eqs. (11), (12), (36), and (37) into Eq.(3), the following equations are obtained:

$$F_x=v_xF_y+E_xt\left(\dot{u}+kw+ks-\frac{t^2k_0}{12}k\right) \tag{38}$$

$$F_y=\frac{E_xt}{1-v_xv_y}[v'+v_x(\dot{u}+kw+ks)]-D_yk_0(v_xk+k_0-w'') \tag{39}$$

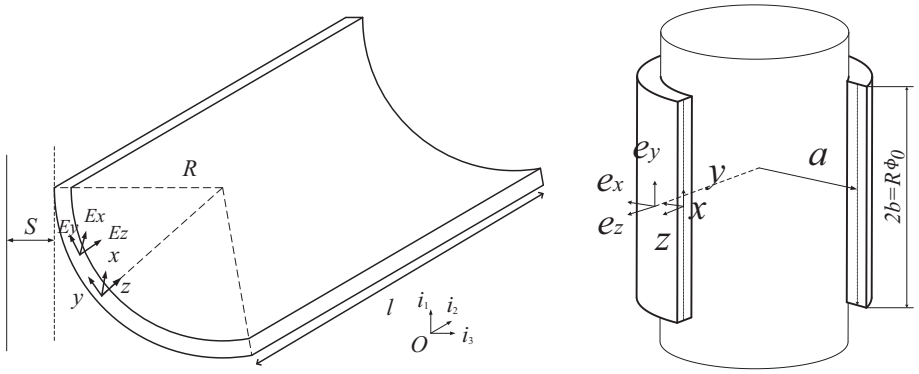

(a) Initial state (b) Deformed state

Fig. 5. Single type II tape spring under bending.

$$N_y = -\frac{\partial M_y}{\partial y} = -\widetilde{D}_y w''' \tag{40}$$

$$\begin{aligned} M_x &= D_x\left[k_0(\dot{u} + kw + v_y v') + k + v_y(k_0 - w'')\right] \\ &= -\tfrac{t^2 k_0}{12} F_x + \widetilde{D}_x\left[k + v_y(k_0 - w'')\right] \end{aligned} \tag{41}$$

$$\begin{aligned} M_y &= -D_y\{v_x k + k_0 - w'' - k_0[v' + v_x(\dot{u} + kw)]\} \\ &= \tfrac{t^2 k_0}{12} F_y - \widetilde{D}_y(v_x k + k_0 - w'') \end{aligned} \tag{42}$$

The single type II tape spring is in pure bending deformed state, and the boundary conditions are expressed as

$$F_y(b) = 0,\ M_y(b) = 0,\ N_y(b) = 0 \tag{43}$$

By substituting Eqs. (38) and (42) into Eq. (15), the following equations are obtained

$$\widetilde{D}_y w''' * * + E_x t k^2\left(w - \frac{t^2 k_0}{12} - \frac{\alpha_{x0}}{k} - s\right) = 0 \tag{44}$$

By combining Eqs. (40) and (42), Eq. (43)can be written as

$$w''(b) = k_0 + v_x k,\ w''(b) = 0 \tag{45}$$

By substituting Eqs. (43) and (44) into Eq. (45), the displacement of the type II tape spring is derived as follows

$$w = \frac{t^2 k_0}{12} - \frac{\alpha_{x0}}{k} - s + \frac{b^2(k_0 + v_x k)}{3}\left(\chi_{11}\sinh\eta\xi\sin\eta\xi - \chi_{12}\cosh\eta\xi\cos\eta\xi\right) \tag{46}$$

The strain energy π_{II} of the type II tape spring can be written as follows

$$\pi_{II} = \frac{k}{2}\int_{-b}^{b} M_x d_y - \frac{k_0}{2}\int_{-b}^{b} M_y d_y \tag{47}$$

By substituting Eqs. (41), (42), and (46) into (47), strain energy π_{II} is derived as

$$\pi_{II} = b\widetilde{D}_x(1 - v_x v_y)k^2 + b\widetilde{D}_y(k_0 + v_x k)^2(1 - A_1) \tag{48}$$

The derivative of strain energy π_{II} with respect to k and the bending moment M_{II} of the type II tape spring can be derived as

$$\begin{aligned} M_{II} &= 2b\widetilde{D}_x(1 - v_x v_y)k + 2b v_x \widetilde{D}_y(k_0 + v_x k)(1 - A_1) \\ &\quad - b\widetilde{D}_y(k_0 + v_x k)^2 \frac{A_4 - A_1}{2k} \end{aligned} \tag{49}$$

The bending moment has no relation to the reverse curvature based on Eq. (49). Both type II and III tape springs are opposite bending senses during the M boom coiling around the hub. Thus, the bending moment of the type III tape spring is similar with the type I tape spring, which is ignored in this section. The deflection of the type II tape spring is different with that of the type I and III tape springs, but all the deflections have no effect on the strain energy. Thus, the theoretical bending moment models of the three types of single tape spring are derived. Then, the bending moment of the M boom is derived.

4. Bending of six tape springs in the M boom

4.1. Geometrical relation

The M boom consists of four tape springs bonding along one longitudinal edge, and the four tape springs are mirror-symmetric. The M boom can be flattened and coiled elastically and self-deploy by releasing stored strain energy around a hub. The marks of the tape springs in the M boom are shown in Fig. 6. The four tape springs in the flattened M boom can be divided into two parts. The inner part consists of four inner side tape springs, including two type I and two type III tape springs. The outer parts

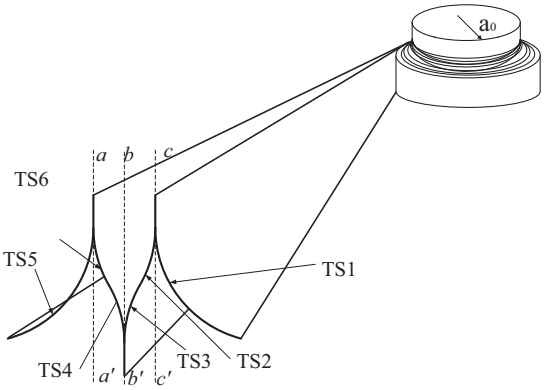

Fig. 6. The marks of tape spring in the M boom.

consist of two type II tape springs. The marks of the type I tape springs are TS3 and TS4. The marks of the type II tape springs are TS1 and TS5. The marks of the type III tape springs are TS2 and TS6. TS3 and TS4 are symmetric about line bb', and TS5 and TS6 are symmetric about line aa'. If the length is ignored, TS1 and TS2 are symmetric about line cc'. What's more, lines aa' and cc' are symmetric about line bb'. Therefore, if TS1 and TS2, and TS5 and TS6 are separately considered as a whole, then the integral tape springs are symmetric about line bb'.

The deformed state geometric diagram of the M boom is shown in Fig. 7. The central curvature of the four tape springs is $k = 1/a_0$, the inner curvature of the inner part is $k_{in} = 1/(a_0 - 2t)$, and the outer curvature of the outer part is $k_{out} = 1/(a_0 + 2t)$.

The central curvature of the inner part is $k_A = 1/(a_0 - t)$, and the inner and outer curvatures of the inner tape spring are $k_1 = 1/(a_0 - 2t)$ and $k_2 = 1/a_0$, respectively. The central curvature of the outer part is $k_B = 1/(a_0 + t)$, and the inner and outer curvatures of the outer tape spring are $k_3 = 1/a_0$ and $k_4 = 1/(a_0 + 2t)$, respectively.

The relationships between the different curvatures are expressed as

$$\begin{cases} k_2 = k_3 = k; \\ k_{in} = k_1 = \frac{k}{1-2tk}; \\ k_{out} = k_4 = \frac{k}{1+2tk}; \\ k_A = \frac{k}{1-kt}; \\ k_B = \frac{k}{1+kt}; \end{cases} \tag{50}$$

where k_1, k_2, k_3 and k_4 represent the curvatures from the inner to outer tape springs.

4.2. Strain energy

On the basis of the derived strain energy of the single tape spring in the previous section, the allocation of strain energy for the M boom (Miyazaki et al., 2015) is given as

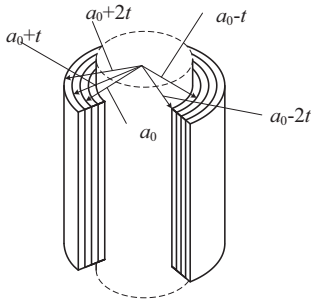

Fig. 7. Deformed state geometric diagram of the M boom.

$$\pi_m = \frac{k}{k_{in}}\pi_{in0} + \frac{k}{k_{out}}\pi_{out0} \tag{51}$$

Where π_{in0} is the strain energy of the inner part, π_{out0} is the strain energy of the inner part, and π_m is the total strain energy of the M boom.

The strain energies π_{m1} of the whole parts of TS5 and TS6 and the TS1 and TS2 are written as

$$\pi_{m1} = \frac{k}{k_{in}}\pi_{in0} + \frac{k}{k_{out}}\pi_{out0} \tag{52}$$

Where π_{in0} represents the strain energy of TS1 and TS2, and π_{out0} represents the strain energy of TS5 and TS6.

Given that TS5 and TS6 are symmetric about line aa' and TS1 and TS2 are symmetric about line cc', the strain energy of the inner and out part can be written as

$$\pi_{in0} = \frac{k_A}{k_1}\pi_{in1} + \frac{k_A}{k_2}\pi_{out1} \tag{53}$$

$$\pi_{out1} = \frac{k_B}{k_3}\pi_{in2} + \frac{k_B}{k_4}\pi_{out2} \tag{54}$$

Where π_{in1} and π_{in2} represent the strain energies of TS1 and TS2, respectively; and π_{out1} and π_{out2} represent the strain energies of the TS5 and TS6, respectively.

By substituting Eqs. (53), (54) and (50) into Eq.(52), π_{m1} is expressed as

$$\begin{aligned}\pi_m &= \tfrac{k}{k_{in}}\left(\tfrac{k_A}{k_1}\pi_{in1} + \tfrac{k_A}{k_2}\pi_{out1}\right) + \tfrac{k}{k_{out}}\left(\tfrac{k_B}{k_3}\pi_{in2} + \tfrac{k_B}{k_4}\pi_{out2}\right)\\ &= \tfrac{(1-2tk)^2}{1-tk}\pi_{in1} + \tfrac{1-2tk}{1-tk}\pi_{out1} + \tfrac{1+2tk}{1+tk}\pi_{in2} + \tfrac{(1+2tk)^2}{1+tk}\pi_{out2}\end{aligned} \tag{55}$$

Given that TS3 and TS4 are symmetric about line bb', the strain energy π_{m2} of the TS3 and TS4 can be written as

$$\pi_{m2} = \frac{k_A}{k_1}\pi_{m3} + \frac{k_A}{k_2}\pi_{out3} \tag{56}$$

Where π_{in3} and π_{out2} represent the strain energies of TS3 and TS4, respectively.

By substituting Eqs. (50) into Eq. (56), π_{m2} is expressed as

$$\pi_{m2} = \frac{k}{k_{in}}\pi_{in3} + \frac{k}{k_{out}}\pi_{out3} = (1-2tk)\pi_{in3} + (1+2tk)\pi_{out3} \tag{57}$$

The total strain energy π_m of the M boom is derived as

$$\pi_{\mathrm{m}} = \pi_{m1} + \pi_{m2} \tag{58}$$

By substituting Eqs. (55) into Eq. (57), π_m is expressed as

$$\begin{aligned}\pi_m = {} & \frac{(1-2tk)^2}{1-tk}\pi_{in1} + \frac{1-2tk}{1-tk}\pi_{out1} + \frac{1+2tk}{1+tk}\pi_{in2}\\ & + \frac{(1+2tk)^2}{1+tk}\pi_{out2} + (1-2tk)\pi_{in3} + (1+2tk)\pi_{out3}\end{aligned} \tag{59}$$

On the basis of Eqs. (31) and (48), the strain energies π_{in1}, π_{out1}, π_{in2}, π_{out2}, π_{in3}, and π_{out3} of respective tape springs TS1, TS2, TS3, TS4, TS5, and TS6 are analyzed as follows.

(i) strain energy π_{in1} consists of a circle with positive curvature k_1, central angle ϕ_2, and a web with width of l. π_{in1} can be expressed as

$$\pi_{in1} = \pi(k_1, b_2, k_0) + \pi(k_1, l, 0) \tag{60}$$

By substituting Eqs. (31) into Eqs. (60), π_{in1} is expressed as

$$\begin{aligned}\pi_{in1} = {} & b_2\widetilde{D}_x(1-v_xv_y)k_1{}^2 + b_2\widetilde{D}_y(k_0+v_xk_1)^2(1-A_1(k_1,b_2,k_0))\\ & + l\widetilde{D}_x(1-v_xv_y)k_1{}^2 + l\widetilde{D}_y(v_xk_1)^2(1-A_1(k_1,l,0))\end{aligned} \tag{61}$$

(ii) strain energies π_{out1} and π_{out3} consist of a circle with negative curvature k, central angle ϕ_1, and a web with width of l. π_{out1} and π_{out3} can be written as

$$\pi_{out1} = \pi_{out3} = \pi(k, b_1, -k_0) + \pi(k, l, 0) \tag{62}$$

By substituting Eqs. (31) into (62), π_{out1} and π_{out3} are expressed as

$$\begin{aligned}\pi_{out1} = \pi_{out3} = {} & b_1\widetilde{D}_x(1-v_xv_y)k^2 + b_1\widetilde{D}_y(-k_0+v_xk)^2(1-A_1(k,b_1,-k_0))\\ & + l\widetilde{D}_x(1-v_xv_y)k^2 + l\widetilde{D}_y(v_xk)^2(1-A_1(k,l,0))\end{aligned} \tag{63}$$

(iii) strain energies π_{in2} and π_{in3} consist of a circle with positive curvature k, central angle ϕ_1, and a web with width of l. π_{in2} and π_{in3} can be written as

$$\pi_{in2} = \pi_{in3} = \pi(k, b_1, k_0) + \pi(k, l, 0) \tag{64}$$

By substituting Eqs. (31) into (62), π_{in2} and π_{in3} are expressed as

$$\begin{aligned}\pi_{in2} = \pi_{in3} = {} & b_1\widetilde{D}_x(1-v_xv_y)k^2 + b_1\widetilde{D}_y(k_0+v_xk)^2(1-A_1(k,b_1,k_0))\\ & + l\widetilde{D}_x(1-v_xv_y)k^2 + l\widetilde{D}_y(v_xk)^2(1-A_1(k,l,0))\end{aligned} \tag{65}$$

(iv) strain energy π_{ou2} consists of a circle with negative curvature k_1, central angle ϕ_2, and a web with width of l. π_{out2} can be written as

$$\pi_{out2} = \pi(k_4, b_2, -k_0) + \pi(k_4, l, 0) \tag{66}$$

By substituting Eq.(31) into Eq.(66), π_{out2} is expressed as

$$\begin{aligned}\pi_{out2} = {} & b_2\widetilde{D}_x(1-v_xv_y)k_4{}^2 + b_2\widetilde{D}_y(-k_0+v_xk_4)^2(1-A_1(k_4,b_2,-k_0))\\ & + l\widetilde{D}_x(1-v_xv_y)k_4{}^2 + l\widetilde{D}_y(v_xk_4)^2(1-A_1(k_4,l,0))\end{aligned} \tag{67}$$

By substituting Eqs. (61), (63), (65) and (67) into Eq. (59), π_m is expressed as

$$\begin{aligned}\pi_m = {} & \tfrac{(1-2tk)^2}{1-tk}\left[b_2\widetilde{D}_xSk_1{}^2 + b_2\widetilde{D}_yP_1{}^2(1-B_{12}) + l\widetilde{D}_xSk_1{}^2 + l\widetilde{D}_y(v_xk_1)^2(1-B_{13})\right]\\ & + (2+tk)\left[b_1\widetilde{D}_xSk^2 + b_1\widetilde{D}_y\widetilde{p}^2(1-B_{01}) + l\widetilde{D}_xSk^2 + l\widetilde{D}_y(v_xk)^2(1-B_{03})\right]\\ & + (2-tk)\left[b_1\widetilde{D}_xSk^2 + b_1\widetilde{D}_yP^2(1-B_{01}) + l\widetilde{D}_xSk^2 + l\widetilde{D}_y(v_xk)^2(1-B_{03})\right]\\ & + \tfrac{(1+2tk)^2}{1+tk}\left[b_2\widetilde{D}_xSk_4{}^2 + b_2\widetilde{D}_y\widetilde{P}_4{}^2(1-B_{42}) + l\widetilde{D}_xSk_4{}^2 + l\widetilde{D}_y(v_xk_4)^2(1-B_{43})\right]\end{aligned} \tag{68}$$

Where

$$B_{12} = A_1(k_1,b_2,k_0) = \tfrac{\cosh 2\eta_{12} - \cos 2\eta_{12}}{\eta_{12}(\sinh 2\eta_{12} + \sin 2\eta_{12})}, \quad B_{13} = A_1(k_1,l,0) = \tfrac{\cosh 2\eta_{13} - \cos 2\eta_{13}}{\eta_{13}(\sinh 2\eta_{13} + \sin 2\eta_{13})} \quad S = 1 - v_xv_y$$

$$P_1 = k_0 + v_xk_1 \quad B_{01} = A_1(k,b_1,k_0) = A_1(k,b_1,-k_0) = \tfrac{\cosh 2\eta_{01} - \cos 2\eta_{01}}{\eta_{01}(\sinh 2\eta_{01} + \sin 2\eta_{01})} \quad \widetilde{P}_1 = -k_0 + v_xk_1$$

$$B_{03} = A_1(k,l,0) = \tfrac{\cosh 2\eta_{03} - \cos 2\eta_{03}}{\eta_{03}(\sinh 2\eta_{03} + \sin 2\eta_{03})} \quad B_{43} = A_1(k_4,l,0) = \tfrac{\cosh 2\eta_{43} - \cos 2\eta_{43}}{\eta_{43}(\sinh 2\eta_{43} + \sin 2\eta_{43})} \quad P = k_0 + v_xk$$

$$\widetilde{P}_4 = -k_0 + v_xk_4 \quad B_{42} = A_1(k_4,b_2,-k_0) = \tfrac{\cosh 2\eta_{42} - \cos 2\eta_{42}}{\eta_{42}(\sinh 2\eta_{42} + \sin 2\eta_{42})} \quad \widetilde{P} = -k_0 + v_xk \quad \eta_{12} = \sqrt[4]{\tfrac{E_xb_2{}^4tk_1{}^2}{4D_y}}$$

$$\eta_{13} = \sqrt[4]{\tfrac{E_xl^4tk_1{}^2}{4D_y}} \quad \eta_{01} = \sqrt[4]{\tfrac{E_xb_1{}^4tk^2}{4D_y}} \quad \eta_{03} = \sqrt[4]{\tfrac{E_xl^4tk^2}{4D_y}} \quad \eta_{43} = \sqrt[4]{\tfrac{E_xl^4tk_4{}^2}{4D_y}} \quad \eta_{42} = \sqrt[4]{\tfrac{E_xb_2{}^4tk_4{}^2}{4D_y}}$$

4.3. Bending moment theoretical modeling

Combined with Eq. (68), and on the basis of the minimum potential energy principle, bending moment M_m can be obtained as follows:

$$M_m = \frac{d\pi_m}{dk} \tag{69}$$

By substituting Eqs. (59) into (69), the following equation can be derived:

$$\begin{aligned} M_m = {} & -2t\pi_{in3} + (1-2tk)M_{in3} + 2t\pi_{out3} + (1+2tk)M_{out3} \\ & + \tfrac{t}{(1+tk)^2}\pi_{in2} + \tfrac{1+2tk}{1+tk}M_{in2} + \tfrac{4(1+tk)^2-1}{(1+tk)^2}t\pi_{out2} + \tfrac{(1+2tk)^2}{1+tk}M_{out2} \\ & \tfrac{1-4(1-tk)^2}{(1-tk)^2}t\pi_{in1} + \tfrac{(1-2tk)^2}{1-tk}M_{in1} + \tfrac{-t}{(1-tk)^2}\pi_{out1} + \tfrac{1-2tk}{1-tk}M_{out1} \end{aligned} \tag{70}$$

Where M_{out1}, M_{in1}, M_{out2}, M_{in2}, M_{out3} and M_{in3} represent the moments corresponding to π_{out1}, π_{in1}, π_{out2}, π_{in2}, π_{out3} and π_{in3}, respectively.

(i) on the basis of Eq. (69), M_{in1}can be written as

$$M_{in1} = \frac{\partial \pi_I}{\partial k_1}\cdot\frac{1}{(1-2tk)^2} = [M(k_1,b_2,k_0) + M(k_1,l,0)]\frac{1}{(1-2tk)^2} \tag{71}$$

By substituting Eqs. (33) into (71), the following equations can be derived

$$\begin{aligned} M_{in1} = {} & \Big[2b_2\widetilde{D}_x(1-v_xv_y)k_1 + 2b_2v_x\widetilde{D}_y(k_0+v_xk_1)(1-A_1(k_1,b_2,k_0)) \\ & -b_2\widetilde{D}_y(k_0+v_xk_1)^2\frac{A_4(k_1,b_2,k_0)-A_1(k_1,b_2,k_0)}{2k_1} \\ & + 2l\widetilde{D}_x(1-v_xv_y)k_1 + 2lv_x\widetilde{D}_y(v_xk_1)(1-A_1(k_1,l,0)) \\ & - 2l\widetilde{D}_y(v_xk_1)^2\frac{A_4(k_1,l,0)-A_1(k_1,l,0)}{4k_1}\Big]\frac{1}{(1-2tk)^2} \end{aligned} \tag{72}$$

(ii) on the basis of Eq. (69), M_{out1} and M_{out3} can be written as

$$M_{out1} = M_{out3} = \frac{\partial\pi_{out1}}{\partial k} = \frac{\partial\pi_{out3}}{\partial k} = M(k,b_1,-k_0) + M(k,l,0) \tag{73}$$

By substituting Eqs. (33) into (71), the following equations can be derived

$$\begin{aligned} M_{out1} = M_{out3} = {} & 2b_1\widetilde{D}_x(1-v_xv_y)k + 2b_1v_x\widetilde{D}_y(-k_0+v_xk)(1-A_1(k,b_1,-k_0)) \\ & -b_1\widetilde{D}_y(-k_0+v_xk)^2\tfrac{A_4(k,b_1,-k_0))-A_1(k,b_1,-k_0))}{2k} \\ & +2l\widetilde{D}_x(1-v_xv_y)k + 2lv_x\widetilde{D}_y(v_xk)(1-A_1(k,l,0)) \\ & -l\widetilde{D}_y(v_xk)^2\tfrac{A_4(k,l,0)-A_1(k,l,0)}{4k} \end{aligned} \tag{74}$$

(iii) on the basis of Eq. (33), M_{in2} and M_{in3} can be written as

$$M_{in2} = M_{in3} = \frac{\partial\pi_{in2}}{\partial k} = \frac{\partial\pi_{in3}}{\partial k} = M(k,b_1,k_0) + M(k,l,0) \tag{75}$$

By substituting Eqs. (49) into (71), the following equations can be derived

$$\begin{aligned} M_{in2} = M_{in3} = {} & 2b_1\widetilde{D}_x(1-v_xv_y)k + 2b_1v_x\widetilde{D}_y(k_0+v_xk)(1-A_1(k,b_1,k_0)) \\ & -b_1\widetilde{D}_y(k_0+v_xk)^2\tfrac{A_4(k,b_1,k_0))-A_1(k,b_1,k_0))}{2k} \\ & +2l\widetilde{D}_x(1-v_xv_y)k + 2lv_x\widetilde{D}_y(v_xk)(1-A_1(k,l,0)) \\ & -l\widetilde{D}_y(v_xk)^2\tfrac{A_4(k,l,0)-A_1(k,l,0)}{2k} \end{aligned} \tag{76}$$

(iv) on the basis of Eq. (33), M_{out2} can be written as

$$M_{out2} = \frac{\partial\pi_{out2}}{\partial k_4}\frac{1}{(1+2tk)^2} = [M(k_4,b_2,-k_0) + M(k_4,l,0)]\frac{1}{(1+2tk)^2} \tag{77}$$

By substituting Eqs. (49) into (71), the following equations can be derived

$$\begin{aligned} M_{out2} = {} & \Big[2b_2\widetilde{D}_x(1-v_xv_y)k_4 + 2b_2v_x\widetilde{D}_y(-k_0+v_xk_4)(1-A_1(k_4,b_2,-k_0)) \\ & -b_2\widetilde{D}_y(-k_0+v_xk_4)^2\frac{A_4(k_4,b_2,-k_0)-A_1(k_4,b_2,-k_0)}{2k_4} \\ & + 2l\widetilde{D}_x(1-v_xv_y)k_4 + 2lv_x\widetilde{D}_y(v_xk_4)(1-A_1(k_4,l,0)) - l\widetilde{D}_y(v_xk_4)^2 \\ & \times\frac{A_4(k_4,l,0)-A_1(k_4,l,0)}{2k_4}\Big]\frac{1}{(1+2tk)^2} \end{aligned} \tag{78}$$

By substituting Eqs. (72), (74), (76) and (78) into (70), the pure bending moment M_m of the M boom can be derived

$$\begin{aligned} M_m = {} & \tfrac{1-4(1-tk)^2}{(1-tk)^2}tJ_{11} + \tfrac{1}{1-tk}J_{12} + \tfrac{2t^3k^2-4t^2k+t}{(1-tk)^2}J_{13} + (2+tk)J_{34} \\ & - \tfrac{2t^3k^2+4t^2k+t}{(1+tk)^2}J_{15} + (2-tk)J_{56} + \tfrac{4(1+tk)^2-1}{(1+tk)^2}tJ_{17} + \tfrac{1}{1+tk}J_{18} \end{aligned} \tag{79}$$

where

$J_{11} = b_2\widetilde{D}_xSk_1{}^2 + b_2\widetilde{D}_yP_1{}^2(1-B_{12}) + l\widetilde{D}_xSk_1{}^2 + l\widetilde{D}_y(v_xk_1)^2(1-B_{13})$, $J_{12} = J_{01} + J_{02}J_{34} = J_{03} + J_{04}$, $J_{02} = 2l\widetilde{D}_xSk_1 + 2lv_x\widetilde{D}_y(v_xk_1)(1-B_{13}) - \zeta_{02}J_{56} = J_{05} + J_{06}$, $J_{01} = 2b_2\widetilde{D}_xSk_1 + 2b_2v_x\widetilde{D}_yP_1(1-B_{12}) - \zeta_{01}$ $J_{13} = b_1\widetilde{D}_xSk^2 + b_1\widetilde{D}_y\widetilde{P}^2(1-B_{01}) + l\widetilde{D}_xSk^2 + l\widetilde{D}_y(v_xk)^2(1-B_{03})$, $J_{03} = 2b_1\widetilde{D}_xSk + 2b_1v_x\widetilde{D}_y\widetilde{P}(1-B_{01}) - \zeta_{03}$, $J_{15} = b_1\widetilde{D}_xSk^2 + b_1\widetilde{D}_yP^2(1-B_{01}) + l\widetilde{D}_xSk^2 + l\widetilde{D}_y(v_xk)^2(1-B_{03})$, $J_{05} = 2b_1\widetilde{D}_xSk + 2b_1v_x\widetilde{D}_yP(1-B_{01}) - \zeta_{05}$, $J_{04} = 2l\widetilde{D}_xSk + 2lv_x\widetilde{D}_y(v_xk)(1-B_{03}) - \zeta_{04}$, $J_{06} = 2l\widetilde{D}_xSk + 2lv_x\widetilde{D}_y(v_xk)(1-B_{03}) - \zeta_{06}$, $J_{89} = J_{08} + J_{09}J_{17} = b_2\widetilde{D}_xSk_4{}^2 + b_2\widetilde{D}_y\widetilde{P}_4{}^2(1-B_{42}) + l\widetilde{D}_xSk_4{}^2 + \zeta_{07}$, $J_{08} = 2b_2\widetilde{D}_xSk_4 + 2b_2v_x\widetilde{D}_y\widetilde{P}_4(1-B_{42}) - \zeta_{08}$, $J_{09} = 2l\widetilde{D}_xSk_4 + 2lv_x\widetilde{D}_y(v_xk_4)(1-B_{43}) - \zeta_{09}$, $\zeta_{01} = b_2\widetilde{D}_yP_1{}^2\frac{C_{12}-B_{12}}{2k_1}$, $\zeta_{02} = l\widetilde{D}_y(v_xk_1)^2\frac{C_{13}-B_{13}}{2k_1}$, $\zeta_{03} = b_1\widetilde{D}_y\widetilde{P}^2\frac{C_{01}-B_{01})}{2k}$, $\zeta_{04} = l\widetilde{D}_y(v_xk)^2\frac{C_{03}-B_{03}}{2k}$, $\zeta_{05} = b_1\widetilde{D}_yP^2\frac{C_{01}-B_{01})}{2k}$, $\zeta_{06} = l\widetilde{D}_y(v_xk)^2\frac{C_{03}-B_{03}}{2k}$, $\zeta_{07} = l\widetilde{D}_y(v_xk_4)^2(1-B_{43})$, $\zeta_{08} = b_2\widetilde{D}_y\widetilde{P}_4{}^2\frac{C_{42}-B_{42}}{2k_4}$, $\zeta_{09} = l\widetilde{D}_y(v_xk_4)^2\frac{C_{43}-B_{43}}{2k_4}$, $C_{12} = \frac{4\sinh2\eta_{12}\sin2\eta_{12}}{(\sinh2\eta_{12}+\sin2\eta_{12})^2}$, $C_{13} = \frac{4\sinh2\eta_{13}\sin2\eta_{13}}{(\sinh2\eta_{13}+\sin2\eta_{13})^2}$, $C_{42} = \frac{4\sinh2\eta_{42}\sin2\eta_{42}}{(\sinh2\eta_{42}+\sin2\eta_{42})^2}$, $C_{43} = \frac{4\sinh2\eta_{43}\sin2\eta_{43}}{(\sinh2\eta_{43}+\sin2\eta_{43})^2}$, $C_{01} = \frac{4\sinh2\eta_{01}\sin2\eta_{01}}{(\sinh2\eta_{01}+\sin2\eta_{01})^2}$, $C_{03} = \frac{4\sinh2\eta_{03}\sin2\eta_{03}}{(\sinh2\eta_{03}+\sin2\eta_{03})^2}$.

4.4. Peak bending moment

The M boom is made by laying four 0.0375-mm-thickness plies $[45°/-45°/-45°/45°]_T$ of T300 carbon fiber reinforced polymer impregnated with epoxy resin, and the thickness of each tape spring is 0.15 mm. The material properties of the M boom are derived based on classical laminated plate theory.

(i) Material parameter of the single ply

The relationship between the stress and strain of the single ply is written as follows:

$$\begin{Bmatrix}\sigma_1\\ \sigma_2\\ \sigma_3\end{Bmatrix} = [\mathbf{Q}]\begin{Bmatrix}\varepsilon_1\\ \varepsilon_2\\ \gamma_{12}\end{Bmatrix} = \begin{bmatrix}Q_{11} & Q_{12} & 0\\ Q_{21} & Q_{22} & 0\\ 0 & 0 & Q_{66}\end{bmatrix}\begin{Bmatrix}\varepsilon_1\\ \varepsilon_2\\ \gamma_{12}\end{Bmatrix} \tag{80}$$

where $[\mathbf{Q}]$ is the reduced stiffness matrix, $Q_{11} = \frac{E_1}{1-v_{12}v_{21}}$, $Q_{12} = Q_{21} = \frac{v_{12}E_2}{1-v_{12}v_{21}} = \frac{v_{21}E_1}{1-v_{12}v_{21}}$, $Q_{22} = \frac{E_2}{1-v_{12}v_{21}}$, $Q_{66} = G$, $v_{21} = \frac{E_2}{E_1}v_{12}$; E_1 and E_2 are the elasticity moduli along the fiber direction and its vertical direction, respectively; G is the shear modulus; and v_{12} and v_{21} are the Passion's ratios.

Given the different ply angles, the relationship between stress and strain must unify to one natural coordinate system. When the main directional coordinate system of the ply material is at arbitrary angle θ with the natural coordinate system, the relationship between stress and strain is changed to

$$\begin{Bmatrix}\sigma_x\\ \sigma_y\\ \sigma_z\end{Bmatrix} = [T]^{-1}[Q]\left([T]^{-1}\right)^T\begin{Bmatrix}\varepsilon_x\\ \varepsilon_x\\ \gamma_{xy}\end{Bmatrix} = \left[\bar{Q}\right]\begin{Bmatrix}\varepsilon_x\\ \varepsilon_x\\ \gamma_{xy}\end{Bmatrix} = \begin{bmatrix}\bar{Q}_{11} & \bar{Q}_{12} & 0\\ \bar{Q}_{21} & \bar{Q}_{22} & 0\\ 0 & 0 & \bar{Q}_{66}\end{bmatrix}\begin{Bmatrix}\varepsilon_x\\ \varepsilon_y\\ \gamma_{xy}\end{Bmatrix} \tag{81}$$

where $[\mathbf{T}] = \begin{bmatrix}\cos^2\theta & \sin^2\theta & 2\sin\theta\cos\theta\\ \sin^2\theta & \cos^2\theta & -2\sin\theta\cos\theta\\ -\sin\theta\cos\theta & \sin\theta\cos\theta & \cos^2\theta-\sin^2\theta\end{bmatrix}$.

Then, the elements in the newly reduced stiffness matrix are written as follows:

$$\begin{cases}\bar{Q}_{11} = Q_{11}\cos^4\theta + 2(Q_{12}+2Q_{66})\sin^2\theta\cos^2\theta + Q_{22}\sin^4\theta\\ \bar{Q}_{12} = (Q_{11}+Q_{22}-4Q_{66})\sin^2\theta\cos^2\theta + Q_{12}\left(\sin^4\theta+\cos^4\theta\right)\\ \bar{Q}_{22} = Q_{11}\sin^4\theta + 2(Q_{12}+2Q_{66})\sin^2\theta\cos^2\theta + Q_{22}\cos^4\theta\\ \bar{Q}_{16} = (Q_{11}-Q_{12}-2Q_{66})\sin\theta\cos^3\theta + (Q_{12}-Q_{22}+2Q_{66})\sin^3\theta\cos\theta\\ \bar{Q}_{26} = (Q_{11}-Q_{12}-2Q_{66})\sin^3\theta\cos\theta + (Q_{12}-Q_{22}+2Q_{66})\sin\theta\cos^3\theta\\ \bar{Q}_{66} = (Q_{11}+Q_{22}-Q_{12}-2Q_{66})\sin^2\theta\cos^2\theta + Q_{66}\left(\sin^4\theta+\cos^4\theta\right)\end{cases} \tag{82}$$

(ii) material parameter of the integral plies

The M boom is made by laying four 0.0375-mm-thickness plies $[45°/\text{-}45°/\text{-}45°/45°]_T$ of T300, which is a symmetrical laminate, and the relationship between the internal force and the strain is as follows:

$$\begin{Bmatrix}N_x\\ N_y\\ N_{xy}\end{Bmatrix} = \begin{bmatrix}A_{11} & A_{12} & 0\\ A_{12} & A_{22} & 0\\ 0 & 0 & A_{66}\end{bmatrix}\begin{bmatrix}\varepsilon_x^0\\ \varepsilon_y^0\\ \gamma_{xy}^0\end{bmatrix} \tag{83}$$

where $A_{ij} = \sum_{k=1}^{n}\left(\bar{Q}_{11}\right)_k(z_k - z_{k-1})$, $t_k = z_k - z_{k-1}$ is the thickness of the kth ply, and the total thickness is t.

The material properties of each ply of the M boom are listed in Table 1. By substituting the material properties into Eq. (80), the converted reduced stiffness matrix is derived as

$$\left[\bar{Q}\right] = \begin{bmatrix}Q_{11} & Q_{12} & 0\\ Q_{21} & Q_{22} & 0\\ 0 & 0 & Q_{66}\end{bmatrix} = \begin{bmatrix}114.53 & 1.77 & 0\\ 1.77 & 5.92 & 0\\ 0 & 0 & 4.5\end{bmatrix} \tag{84}$$

By substituting Eqs. (84) into (82), $\left[\bar{Q}\right]_k$ can be derived. Then, it is substituted into Eq. (83), and the relationship between the internal force and the strain is derived as

$$\begin{Bmatrix}N_x\\ N_y\\ N_{xy}\end{Bmatrix} = \begin{bmatrix}35.54t & 26.50t & 0\\ 26.50t & 35.54t & 0\\ 0 & 0 & 29.67t\end{bmatrix}\begin{bmatrix}\varepsilon_x^0\\ \varepsilon_y^0\\ \gamma_{xy}^0\end{bmatrix} \tag{101}$$

Then, the integral elasticity modulus of the M boom can be derived as $E_x = E_y =$ 34.99Gpa. The geometrical parameters of the M boom are b_1 = 5 mm, b_2 = 15 mm, l = 5 mm, R = 20 mm and t = 0.15 mm which are substituted into Eq. (79). The theoretical peak bending moment M_m^T of the M boom is derived as

$$M_m^T = M_m|_{\max} = 0.33\text{Nm}$$

5. Experimental evaluation

The M boom samples and the experimental equipment were processed. The experimental equipment is shown in Fig. 8. One end of the M boom was clamped at the hub. The push–pull gauge was used to measure the peak bending force at the end of the rod, and the other end was fixed to the axis of the hub. The M boom was a thin-walled structure, which is difficult to manufacture. The single tape spring with one web was processed. Then the four tape springs were bonded together in a vacuum chamber. The two M−boom samples were developed first. The other two M−boom samples were fabricated by modified processing method because some crack was appeared when the M booms were bended several times. The four M booms are shown in Fig. 9. Average bending peak force $\bar{F}_b$ multiplies by the length l_r = 0.108 m of the arm to derive the bending peak moment M_m^p of the M boom.

The curve of the bending force versus the experimental time for one measurement is shown in Fig. 10. The bending force first increases to a peak value of 3.10 N and then suddenly reduces to a stable value. The bending force value of the four M booms was tested 20 times. The peak bending force during one measurement is shown in Fig. 11, and the bending force values F_b in 20 measurements are listed in Table 2.

According to Table 2, average bending peak force $\bar{F}_b$ is 3.043 N. Then, the average bending peak moment M_m^p of experiment is derived as 0.32869 Nm. Theoretical bending peak moment M_m is 0.33Nm based on the bending moment theoretical model in Section 4. The relative error between the theoretical and experimental results of the peak bending moment is −0.396%, verifying the accuracy of the theoretical model. The discrepancy can be attributed to the start of the M boom's bending from the completely natural status in the theoretical modeling, but one end of the M boom is flattened before the push–pull gauge is measured in the test, and the fibers are broken and failed after the M boom wrapped around the hub many times, reducing the bending stiffness and the peak bending moment.

Table 1
Material properties of the single ply T300.

Material properties	Values
Longitudinal stiffness E_1/GPa	114
Transverse stiffness E_2/GPa	5.89
Shear stiffness G/GPa	4.5
Poisson's ratio v	0.3
Density ρ/kg/m^3	2500

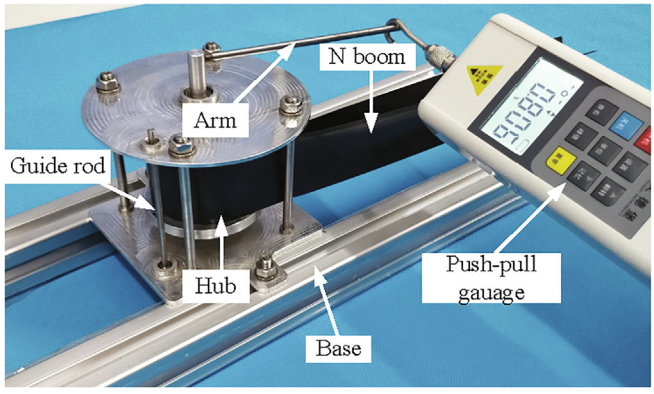

Fig. 8. Experimental equipment.

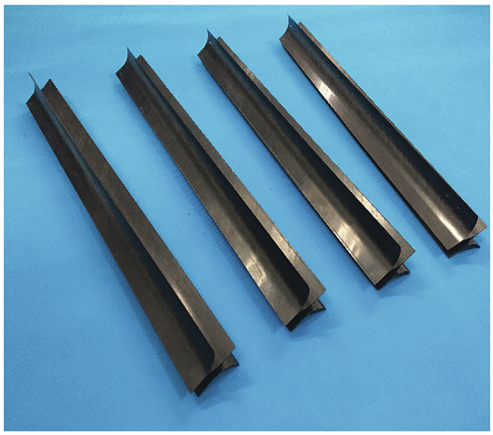

Fig. 9. Four M booms.

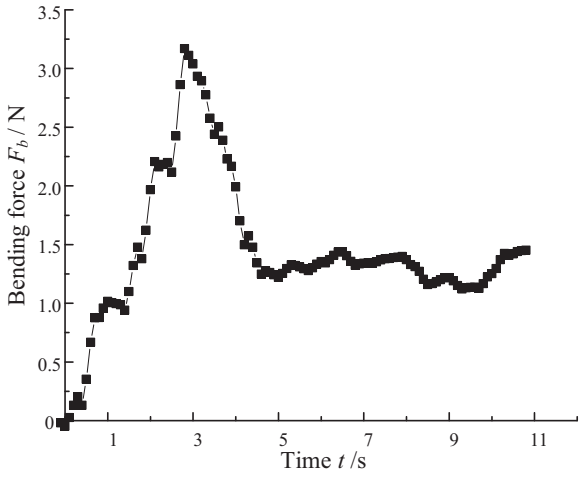

Fig. 10. Curve of the bending force vs. the experimental time for one measurement.

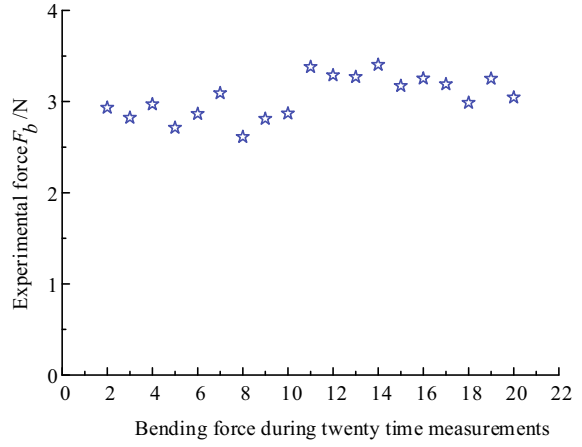

Fig. 11. Bending force during twenty time measurements.

6. Conclusions

The covariant base vectors of the geometrical relation of the single tape spring was analyzed by establishing three coordinate systems. The constitutive relation of the single tape spring between stress and strain was expressed based on the Kirchhoff-Love hypothesis. The equilibrium and controlling equations of the single tape spring were modeled based on Calladine shell theory. Then the strain energy of the single tape spring was modeled by integration.

The strain energies of each type tape spring were derived by the method for single tape springs. The total strain energy of the M boom was calculated by the sum of those of different type tape springs. The closed-form expression of the bending moment model of the M boom was established based on the minimum potential energy principle and the peak bending moment was derived by maximizing the theoretical model of the bending moment.

The four M−boom samples and the experimental equipment were processed. The peak bending moment of the M boom can be derived by 20 measurements of the samples. The experimental and theoretical peak bending moments are 0.32869 and 0.33Nm, respectively. The relative error between the theoretical and experimental results is −0.396% validating the accuracy of the theoretical model for the peak bending moment of the M boom.

The theoretical model derived in this article can be applied to obtain the bending deformation and peak bending moment of the tape springs and the M booms. In addition, the theory is of great important for designing membrane deployable structures.

Table 2
Bending force values of 20 measurements.

Sample code	Number	Peak force F_b/N	Peak bending moment M_m^p/Nm
M−1	1	2.948	0.3184
	2	2.933	0.3168
	3	2.823	0.3048
	4	2.969	0.3049
	5	2.713	0.2930
M−2	1	2.864	0.3093
	2	3.093	0.3340
	3	2.611	0.2820
	4	2.812	0.3037
	5	2.869	0.3089
M−3	1	3.380	0.371
	2	3.289	0.361
	3	3.269	0.359
	4	3.403	0.374
	5	3.171	0.348
M−4	1	3.253	0.357
	2	3.189	0.351
	3	2.986	0.328
	4	3.250	0.357
	5	3.044	0.335

Acknowledgements

This study was co-supported by the Key Funds of the National Natural Science Foundation of China, China (No. 51835002), the National Natural Science Foundation of China, China (No. 51975001), in part by the Joint Funds of the National Natural Science Foundation of China (No. U1637207) and the Key Research and Development Plan of Anhui Province, China (No. 201904A05020034).

References

Bai, J.B., Chen, D., Xiong, J.X., Shenoi, R.A., 2019. Folding analysis for thin-walled deployable composite boom. Acta. Astronaut. 159, 622–636.
Bessa, M.A., Pellegrino, S., 2018. Design of ultra-thin shell structures in the stochastic post-buckling range using Bayesian machine learning and optimization. Int. J. Solids. Struct. 139–140, 174–188.
Chu, Z.Y., Lei, Y.A., 2014. Design theory and dynamic analysis of a deployable boom. Mech. Mach. Theory. 71, 126–141.
Fernandez, J.M., Visagie, L., Schenk, M., Srohlman, O.R., Aglietti, G.S., Lappas, V.J., Erb, S., 2014. Design and development of a gossamer sail system for deorbiting in low earth orbit. Acta. Astronaut. 103, 204–225.

Fukunaga, M., Miyazaki, Y., 2018. Structural characteristics of self-extensible boom, AIAA SciTech Forum, 8–12 January 2018. Kissimmee, Florida.
Hoang, B., White, S., Spence, B., Kiefer, S., 2016. Commercialization of Deployable Space Systems' roll-out solar array (ROSA) technology for Space Systems Loral (SSL) solar arrays. Aerospace Conf. IEEE.
Hoskin, A., Viquerat, A., Aglietti, G.S., 2017. Tip force during blossoming of coiled deployable booms. Int. J. Solids. Struct. 118–119, 58–69.
Hu, Y., Chen, W.J., Gao, J.F., Hu, J.H., Fang, G.Q., Peng, F.J., 2017. A study of flattening process of deployable composite thin-walled lenticular tubes under compression and tension. Compos. Struct. 168, 164–177.
Johnson, L., Whorton, M., Heaton, A., Pinson, R., Laue, G., Adams, C., 2011. Nanosail-D: a solar sail demonstration mission. Acta. Astronaut. 68, 571–575.
Lane, S.A., Murphey, T.W., Zatman, M., 2011. Overview of the innovative space-based radar antenna technology program. J. Spacecraft. Rockets 48 (1), 135–145.
Mallikarachchi, H.M.Y.C., Pellegrino, S., 2014b Design of ultrathin composite self-deployable booms. J, Spacecr. Rocket., 51(6): 1811–1821.
Mallikarachchi, H.M.Y.C., Pellegrino, S., 2014. Deployment dynamics of ultrathin composite booms with tape-spring hinges. J. Spacecr. Rocket. 51 (2), 604–613.
Miyazaki, Y., Inoue, S., Tamura, Y., 2015. Analytical solution of the bending of a bi-convex boom. Mech. Eng. J. 2 (6), 1–19.
Oberst, S., Tuttle, S.L., Griffin, D., Lambert, A., Boyce, R.R., 2018. Experimental validation of tape springs to be used as thin-walled space structures. J. Sound. Vib. 419, 558–570.
Seffen, K.A., Pellegrino, S., 1999. Deployment dynamics of tape springs. Proc. R. Soc. Lond. A. 455, 1003–1048.
Yang, H., Guo, H.W., Wang, Y., Liu, R.Q., Li, M., 2018. Design and experiment of triangular prism mast with tape-spring hyperelastic hinges. Chin. J. Mech. Eng. 31, 33.
Yang, H., Liu, L., Guo, H.W., Lu, F.S., Liu, Y.B., 2019. Wrapping dynamic analysis and optimization of deployable composite triangular rollable and collapsible booms 59 (4), 1371–1383.